Biochimica et Biophysica Acta 1838 (2014) 3118–3129

Contents lists available at ScienceDirect

Biochimica et Biophysica Acta

journal homepage: www.elsevier.com/locate/bbamem

Effects of cargo molecules on membrane perturbation caused by transportan10 based cell-penetrating peptides

Luís Vasconcelos [a,*,1], Fatemeh Madani [a,1], Piret Arukuusk [b], Ly Pärnaste [b], Astrid Gräslund [c], Ülo Langel [a,b]

[a] Department of Neurochemistry, Arrhenius Laboratories for Natural Sciences, Stockholm University, Sweden
[b] Laboratory of Molecular Biotechnology, Institute of Technology, University of Tartu, Estonia
[c] Department of Biochemistry and Biophysics, Arrhenius Laboratories for Natural Sciences, Stockholm University, Sweden

ARTICLE INFO

Article history:
Received 19 March 2014
Received in revised form 30 July 2014
Accepted 8 August 2014
Available online 15 August 2014

Keywords:
Cell-penetrating peptide
Large unilamellar vesicle
Membrane perturbation
Endosomal escape
NickFect
PepFect

ABSTRACT

Cell-penetrating peptides with the ability to escape endosomes and reach the target are of great value as delivery vectors for different bioactive cargoes and future treatment of human diseases. We have studied two such peptides, NickFect1 and NickFect51, both originated from stearylated transportan10 (PF3). To obtain more insight into the mechanism(s) of peptide delivery and the biophysical properties of an efficient vector system, we investigated the effect of different bioactive oligonucleotide cargoes on peptide–membrane perturbation and peptide structural induction. We studied the membrane interactions of the peptides with large unilamellar vesicles and compared their effects with parent peptides transportan10 and PF3. In addition, cellular uptake and peptide-mediated oligonucleotide delivery were analyzed. Calcein leakage experiments showed that similar to transportan10, NickFect51 caused a significant degree of membrane leakage, whereas NickFect1, similar to PF3, was less membrane perturbing. The results are in agreement with previously published results indicating that NickFect51 is a more efficient endosomal escaper. However, the presence of a large cargo like plasmid DNA inhibited NickFect's membrane perturbation and cellular uptake efficiency of the peptide was reduced. We conclude that the pathway for cellular uptake of peptide complexes is cargo dependent, whereas the endosomal escape efficacy depends on peptide hydrophobicity and chemical structure. For small interfering RNA delivery, NickFect51 appears to be optimal. The biophysical signature shows that the peptide alone causes membrane perturbation, but the cargo complex does not. These two biophysical characteristics of the peptide and its cargo complex may be the signature of an efficient delivery vector system.

1. Introduction

The possibility of selectively and efficiently manipulating eukaryotic gene expression holds much promise for modern medicine. Research has been focused on finding new stable biomolecules and their synthetic analogs that can correct or substitute disease causing genetic information. Among the candidates are nucleic acids, such as double-stranded plasmid DNA (pDNA) [1,2], short single-stranded splice-correcting oligonucleotides (SCO) [3,4] and small interfering RNA (siRNA) [5,6]. Although some recent cases of success can be pointed out [7] the use of these nucleic acid based therapies in clinical applications is limited until present by the poor stability in serum containing media and low uptake into cells due to their high molecular weight, negative charge and hydrophilic nature.

The use of cell-penetrating peptides (CPPs) as delivery vehicles for biomolecular cargoes, such as pDNA, SCOs and siRNAs, offers a set of advantages such as low toxicity and efficiency at reduced doses and some of these peptides are able to promote endosomal escape after cell internalization [8–10]. Generally, CPPs are defined as short and water-soluble peptides, which can be hydrophilic (cationic), hydrophobic or intermediately hydrophobic [11,12]. A major advantage of some CPPs is their capacity of forming stable non-covalent complexes with the cargo [13]. However this strategy often results in entrapment of the CPP/cargo complexes in endosomal vesicles after cellular uptake by endocytosis [14–16]. The necessity to improve endosomal escape has driven the insertion of several chemical modifications to CPPs, such as the addition of trifluoromethylquinoline moieties or replacing certain residues with His to make endosomolytic CPPs [6,17–19].

Abbreviations: CPP, cell-penetrating peptide; TP10, transportan10; NickFect, NF; PepFect, PF; FACS, fluorescence activated cell sorting; POPC, palmitoyl-2-oleoyl-phosphatidylcholine; POPG, palmitoyl-2-oleoyl-phosphatidylglycerol; LUV, large unilamellar vesicle; CD, circular dichroism; MR, molar ratio; CR, charge ratio; DLS, dynamic light scattering; SCO, splice-correcting oligonucleotide; pDNA, plasmid DNA; siRNA, small interfering RNA; pGL3, luciferase expressing plasmid; FAM, carboxyfluorescein

* Corresponding author at: Stockholm University, Department of Neurochemistry, Svante Arrheniusv 16B, SE-106 91 Stockholm, Sweden. Tel.: +46 8 16 41 96.
E-mail address: luis@neurochem.su.se (L. Vasconcelos).

[1] These authors contributed equally to this work.

http://dx.doi.org/10.1016/j.bbamem.2014.08.011
0005-2736/

Transportan10 (TP10) is one of the well-known CPPs, a truncated analog of transportan with the N-terminal fragment from the galanin neuropeptide and the C-terminal fragment from the wasp venom peptide mastoparan and an extra lysine positioned between the two fused sequences [20–22]. It belongs to a group of the hydrophobic CPPs with strong affinity to a model membrane already at low concentrations [11]. TP10 showed not only high transduction efficiency but also high cell toxicity [23].

Various TP10 analogs have been developed with the objective to increase the bioavailability, stability and efficiency in cargo delivery. TP10 was modified with stearic acid and gave origin to a new family of stearylated CPPs, named PepFects (PFs). PepFect3 (PF3) is the closest TP10 analog with only an additional stearyl moiety at the N-terminus, allowing the formation of stable peptide/oligonucleotide complexes [4,24]. It has been shown that PF3 has lower affinity for a model membrane compared to unstearylated TP10 [25]. The other family of stearylated TP10 analogs is named NickFects. NickFect1 (NF1) resulted from the replacement of isoleucine8 by a more hydrophilic threonine, and additionally the insertion of a phosphoryl group to tyrosine3 in the stearylated TP10 (PF3) sequence. These modifications increase its hydrophilicity and reduce its charge leading to a pH-dependent peptide vector with a good endosomolytic capacity [26–28]. NickFect51 (NF51) has a kink resulted from two simultaneous modifications to PF3, namely the replacement of lysine7 with ornithine and the use of δ-NH_2 group of ornithine7 for subsequent synthesis instead of α-NH_2 (Table 1). This modification enhances the stability of the complexes in the cytosol and their endosomal escape [29–31]. It has been also found that NF51 functions as an efficient CPP in protein production system [27].

The number of CPPs is increasing including both protein-derived and designed peptides with different physico-chemical properties [32]. However, there is still space for improvement regarding the efficacy of CPPs in the presence of serum as well as to enhance their endosomal escape and biological activities [33]. In addition, both the cellular internalization and endosomal escape mechanisms of CPPs are not well understood. Understanding the molecular mechanisms underlying the CPP cellular uptake and membrane translocation is a necessary prerequisite to characterize the structural basis for modulation of these peptides. Although several parameters may simultaneously affect their biological responses, phospholipid–membrane interaction plays a major role in their cellular uptake and endosomal escape efficiencies and hence their biological activities.

It should be emphasized that the presence of cargo can alter the mechanism of internalization as well as endosomal escape efficiency. Cargo characteristics such as size, charge and conjugation methodology have been shown to influence the CPP translocation mechanism [17,34–38]. However there are few studies concerning the effect of cargo on CPP–membrane interaction and perturbation. One of these studies showed that streptavidin protein covalently bound to TP10 significantly decreases the amount of leakage caused by the peptide while smaller cargo has no obvious effect on peptide–membrane perturbation [39]. In 2002, Fischer et al. [37] evaluated CPPs for the controlled import of small molecules. They studied the dependence of the CPP driven import efficiency for different conjugated fluorophores and for the nature of cargo. They have reported an independence of the nature of the fluorophore contrasted by a marked dependence of the peptide cargo [37]. More recently, Freire et al. [40] developed a novel mathematical lipid partition model, which allows estimating lipid–water partition constants of supramolecular CPP–cargo complexes from fluorescence spectroscopy data. In their work they tested the partition extent of two membrane active peptides derived from dengue virus capsid protein (DENV C protein) with potential CPP properties, both free and in the presence of ssDNA molecular cargo. According to the authors, deducing carrier properties from studies using free CPPs is limited, due to the structural and chemical rearrangements revealed when part of supramolecular complexes [40].

This work aims to investigate the membrane bilayer interaction of three different TP10 analogs, PF3, NF1 and NF51, in the presence or absence of a cargo. These TP10 modified peptides have shown different biological activities when they are non-covalently attached to cargo molecules [4,26,27]. An obvious question is what variables could drive the membrane interaction of CPP and CPP/cargo complexes, enhance the membrane perturbation and therefore make them more efficient delivery vectors.

We employed large unilamellar vesicles (LUVs) as a bio-membrane model system to study the abovementioned peptides. LUVs are a simplified and relevant membrane mimetic system for studying peptide–membrane interaction and peptide structure induction in the presence of the membrane. Both neutral vesicles composed of zwitterionic POPC and partially negatively charged vesicles composed of POPC/POPG (7:3) phospholipids were used. Three different spectroscopic methods were used including fluorescence spectroscopy to investigate peptide induced membrane leakage, circular dichroism (CD) spectroscopy to evaluate secondary structure induction and dynamic light scattering (DLS) to measure the evolution of size. Surface charge using zeta-potential was also measured for the pure peptide and peptide/cargo complexes in water solution. Besides biophysical techniques, we studied the impact of the cargo on the peptide ability to gain intracellular access utilizing fluorescence activated cell sorting (FACS) on live cells. In addition, functional assays were used to evaluate and compare their potentials in delivery of biomolecules. Altogether, the results may

Table 1
Peptides and the respective cargo complexes investigated in this work together with their physico-chemical properties.

CPP	PF3	NF1	NF51
Sequence[a]	Stearyl-AGYLLGKINLKALAALAKKIL[b]	Stearyl-AGY(PO_3)LLGKTNLKALAALAKKIL[b]	Stearyl-AGYLLG)δ-OINLKALAALAKKIL[b]
Average hydrophobicity[c]	0.95	0.35	0.99
Positive charge	4	3	4
Concentration (μM)[d]	5	8	2
CPP/pGL3			
CR[e]	(3:1)	(3:1)	(3:1)
MR	(7200:1)	(7200:1)	(7200:1)
CPP/SCO			
CR	(2:1)	(1.5:1)	(2:1)
MR	(10:1)	(10:1)	(10:1)
CPP/siRNA			
CR	(2:1)	(1.5:1)	(2:1)
MR	(20:1)	(20:1)	(20:1)

[a] All peptides are N-terminally stearylated (stearyl stands for $CH_3(CH_2)_{16}CO-$).
[b] All peptides have amidated C-terminus and peptides used for cellular uptake experiments were labeled with FAM to ε-NH_2 group of additional lysine at the C-terminus.
[c] Average amino acid hydrophobicity was calculated according to [40,44].
[d] Based on the peptide potency in leakage induction, different peptide concentrations were used for peptide/cargo complex preparation in the leakage and CD experiments.
[e] CR and MR refer to charge ratio and molar ratio, respectively.

suggest the crucial CPP characteristics required for cellular delivery leading to the design of an optimized CPP.

2. Materials and methods

2.1. Materials

Zwitterionic 1-palmitoyl-2-oleoyl-*sn*-glycero-3-phosphocholine (POPC) and 1-palmitoyl-2-oleoyl-*sn*-glycero-3[phospho-rac-(1-glycerol)] with a negative head group at neutral pH (POPG) were purchased from Avanti Polar Lipids (Alabaster, Alabama, USA) and were used without further purification. Calcein, a fluorescein derivative ($C_{30}H_{26}N_2O_{13}$, 622.5 Da) was obtained from Molecular Probes, The Netherlands. PD-10 desalting columns were obtained from GE Healthcare (Buckinghamshire, UK). Triton X-100 was purchased from Sigma-Aldrich. PS-2-OMe SCO (5-CCU CUU ACC UCA GUU ACA-3) was purchased from RiboTask (Denmark), pGL3 Luciferase Reporter Vector was purchased from Promega (Sweden) and Luciferase siRNA (Sense 3′-TTU AUG CUG CCA UGC AUG CUA-5′, AntiSense 5′-AUA CGA CGG UAC GUA CGA UTT-3) was a kind gift from Doctor Glynn Williams at GSK Medicines Research Center.

2.2. Peptide synthesis

Peptides used in this study (Table 1) were chemically synthesized on an automated peptide synthesizer (Applied Biosystems, USA) using Rinkamide 4-methylbenzhydrylamine resin (0.452 mmol/g, IRIS Biotech, Germany) to obtain C-terminally amidated peptides using standard fluorenylmethyloxycarbonyl (Fmoc) solid-phase peptide synthesis strategy. Reaction was carried out using HOBT/HBTU as coupling reagents in DMF with DIEA as an activator base. For NF51 Boc-L-Orn(Fmoc)-OH (Bachem, Germany) and for NF1 Fmoc-Tyr(PO_3H_2)-OH (Bachem, Germany) were used. Stearylation was performed by manually coupling the stearic acid to the N-terminus of the peptide overnight, at room temperature with 5 equivalent of stearic acid. For carboxyfluorescein (FAM) labeled peptides, 5,6-carboxyfluorescein was coupled on-resin to ε-NH_2 group of additional lysine at the C-terminus of peptides. After cleavage (H_2O/TIS/TFA 2.5/2.5/95 (v/v)) and precipitation on cold ether, peptides were purified by reversed-phase high-performance liquid chromatography (RP-HPLC), with a C4 preparative column (250 × 10 mm, Phenomenex Jupiter), running a gradient of ACN/H_2O (0.1% TFA). Purified peptides were analyzed by MALDI-TOF MS using alpha-cyano-4-hydroxy-cinnamic acid (α-CHCA) as crystallization matrix (Voyager-DE STR, Applied Biosystems). MALDI-TOF MS: NF51: 2434 (calcd: 2434); FAM-NF51: 2921 (calcd: 2921); NF1: 2516 (calcd: 2514); FAM-NF1: 3003 (calcd: 3001); PF3: 2448 (calcd: 2448); FAM-PF3: 2934 (calcd: 2934).

2.3. Preparation of large unilamellar vesicles

Neutral and anionic large unilamellar vesicles were prepared by dissolving phospholipids (zwitterionic POPC and 30% negatively charged POPG) at the desired concentration in chloroform to obtain a homogeneous solution. Then the solvent was removed by evaporating under high vacuum for at least 3 h. The resulting dried lipid film was re-suspended by addition of 50 mM potassium phosphate buffer solution (pH 7.4) followed by 10 min of vortexing. Five freeze–thaw cycles were applied to the solution to reduce the lamellarity. Next, the lipid solution was pushed through two polycarbonate filters (100 nm pore size) 20 times by using an Avanti manual extruder. This method gave unilamellar vesicles with 100 nm diameter [41]. Dynamic light scattering (DLS) was used to examine the size and stability of the vesicles.

2.4. Calcein release from large unilamellar vesicles

Large unilamellar vesicles (LUVs) with entrapped fluorophore and calcein were prepared by using 50 mM potassium phosphate buffer solution containing 55 mM calcein with the previously mentioned method. The final pH was adjusted to 7.4. Free calcein outside the vesicles was removed by passing through Sephadex-G25 columns two times. The fluorescence intensity of calcein with different CPPs was recorded on a Horiba Jobin Yvon Fluorolog-3 spectrofluorometer using 490 nm excitation and 517 nm emission wavelengths at 20 °C. The fluorescence intensity in the presence of 55 mM calcein is low due to self-quenching, but increases upon dilution. The release of calcein was monitored as an increase in the fluorescence intensity at various peptide incubation time points. The vesicle solution was treated with 10% (w/v) Triton X-100 to induce 100% calcein leakage. Using this as a reference and by subtracting the background fluorescence, the degree of calcein leakage induced by different peptides was calculated using the following equation: % calcein leakage $= [(F - F_0) / (F_r - F_0)] \times 100$, where F_0 and F_r are the initial fluorescence intensities observed without peptide and after treatment with Triton X-100, respectively. F is the fluorescence intensity in the presence of CPPs (or CPP/cargo complexes). The standard deviation in the endpoints (10 min) was less than ±10 in units of % calcein leakage.

2.5. Preparation of CPP/cargo complexes

To prepare CPP/cargo complexes, cargo was mixed with the CPP in water by repeated pipetting and incubated at room temperature for 30 min. The charge ratio (CR) of the CPP to the pGL3 was calculated taking into account the positive charges of the CPP and negative charges of pGL3. Complexes with SCO and siRNA in water were prepared with different molar ratios (MR) corresponding to the amount of moles of the CPP and the cargo (Table 1). The ratio between the peptide and cargo was based on previously published data where the efficiency of in vitro transfection was shown to be optimal [4,26,27].

2.6. Zeta-potential measurements

Surface charges of the complexes (zeta-potentials) were measured in water using a Malvern Zetasizer Nano (ZS) instrument. CPP/cargo complexes were prepared as described in the previous section. Each solution was temperature-equilibrated to 20 °C for 1 min in a zeta cell.

2.7. Dynamic light scattering (DLS)

DLS was used to determine the hydrodynamic radius of the vesicles in the presence and absence of CPPs (or CPP/cargo complexes). Measurements were carried out using a light scattering instrument ALV/CGS-3 equipped with a Light Scattering Electronics and Multiple Tau Digital correlator ALV/LSE-5004. Correlation data were acquired typically for 3 runs each for 30 s. Correlation functions at 150° were recorded at a temperature of 20 °C using a Julabo temperature control. Data analysis was performed using a nonlinear fit model via ALV-regularized Fit from the AVL Correlator Software for Windows, version 3.0 (ALV GmbH, Langen, Germany). ALV-NonLin Data Analysis fits an integral type model function to the correlation function using the CONTIN 2DP constrained regularization method [42,43]. Unweighted (intensity-weighted) particle size distributions were obtained by fitting data with the CONTIN 2DP routine [42], presented in the ALV data analysis package.

2.8. Circular dichroism measurements

Circular dichroism (CD) was used to determine the secondary structure of the CPPs in complex with the cargoes in buffer and also in the presence of the phospholipid membrane. CD spectra were recorded on

a Chirascan CD spectrometer at 20 °C. Wavelengths between 190 nm and 260 nm were recorded, using a bandwidth of 0.5 nm. A quartz cuvette with an optical path length of 4 mm was used, requiring approximately 1 ml of sample. The temperature was adjusted using a TC 125 temperature control. The background spectra of the vesicle solution were subtracted from the peptide spectra. Spectra were collected and averaged over 10 measurements.

2.9. Fluorescence activated cell sorting (FACS) analysis to measure cellular uptake

5×10^4 of HeLa cells were seeded 24 h prior to experiments onto 24-well plates using Dulbecco's Modified Eagle Medium (DMEM) supplemented with 0.1 mM non-essential amino acids, 10% fetal bovine serum, 100 U/ml penicillin and 100 mg/ml streptomycin. Cells were treated with FAM-CPP or FAM-CPP/cargo complexes for indicated times. Thereafter media was removed, cells were rinsed with phosphate buffered saline (PBS) and detached from the plate using trypsin/EDTA in PBS for 5 min at 37 °C. Cells were suspended with PBS containing 5% fetal bovine serum (FBS). Flow cytometry analysis was carried out on a BD LSRII flow cytometer (BD Biosciences) and the population of viable cells was determined from a scatter plot: forward scattered light (FSC) vs. side scattered light (SSC). A minimum of 10,000 events from the viable cell population per sample were analyzed.

2.10. Biological activity of transfected cargo to measure transfection efficiency

4×10^4 HeLa cells or 5×10^4 HeLa pLuc 705 cells were seeded 24 h before the experiment into 24-well plates to reach 75% confluence on the day of transfection. For pDNA transfection HeLa cells and for SCO transfection HeLa pLuc705 cells were utilized.

To determine siRNA intracellular delivery, HeLa cells were first transfected with BES PX plasmid, containing luc2 gene using Lipofectamine 2000 for 3 h according to the manufacturer's protocol, followed by replacement of the medium with fresh serum-containing medium to avoid toxic effects and treated with CPP/siRNA complexes 24 h post-transfection with luc2 plasmid.

Cells were treated with preformed complexes for 24 h in serum-containing medium, washed with PBS and lysed using 100 μl 0.1% Triton X-100 in PBS buffer for 30 min at 4 °C. Luciferase activity was measured using Promega's luciferase assay system on a GLOMAX™ 96 microplate luminometer (Promega, Sweden). Data was normalized to protein content measured with a DC protein determination kit (Bio-Rad Laboratories, Inc., USA). Lipofectamine 2000 and LF RNAiMax as positive controls were used according to the manufacturer's protocol.

2.11. Cell viability measurements

Cell viability was analyzed by CytoTox-Glo™ Assay (Promega, Sweden). 10,000 HeLa cells were seeded into 96-well plates 24 h before the experiment. Complexes were formed as described or peptide solution in MQ was made 10× of given concentration. 100 μl of serum-containing medium was added to cells. 24 h after treatment the number of dead cells and total cells was measured on the GLOMAX™ 96 microplate luminometer. Results are given as % of live cells (viability).

3. Results

In the present work, the phospholipid membrane interactions and conformational properties of three TP10 derivative peptides were investigated (Table 1). In addition, we studied the impact of the presence of cargo molecules, non-covalently attached to the peptide, on the peptide–membrane interaction, membrane perturbation as well as the peptide cellular uptake efficiency. We have used three types of cargoes, which are distinct in their size, structure and number of negative charges. The Firefly Luciferase SCO RNA is single-stranded with 18 base pairs and 18 negative charges, the Firefly Luciferase siRNA is double-stranded with 21 base pairs resulting in 42 negative charges and finally the pGL3 is a 5256 base pair circular plasmid DNA molecule which is highly negatively charged. Functional assays were performed to compare biological activities of peptides and evaluate their endosomal escape efficiencies. Table 1 summarizes the investigated peptides and the respective cargo complexes.

In membrane leakage experiments, several peptide treatment concentrations were used for all investigated CPPs depending on their potent membrane interactions. For comparison, we included the parent peptide, TP10, in leakage and CD experiments. For CPP/cargo complex preparation, we have chosen a suitable peptide concentration that induces observable while low leakage (less than 50%) for each peptide. Due to different peptide potencies in leakage induction, the peptide treatment concentration used for complex preparation was not the same for the investigated peptides (Table 1). In all experiments, the selected peptide to cargo ratio was based on previously published data where the efficiency of in vitro transfection was shown to be optimal [4,26,27]. We used an optimal charge ratio (CR3) for the CPP/plasmid complex and an optimal molar ratio (MR10 and MR20) for CPP/SCO and CPP/siRNA complexes, respectively (Table 1). In cellular assays, the same CPP/cargo ratios were used but to avoid cellular toxicity, cells were treated with lower peptide concentrations. Cell viability upon treatment with peptide/cargo complexes was measured with CytoTox-Glo™ assay (Fig. S9A and B).

3.1. Peptide interaction with the model membrane

The membrane perturbing effects of the peptides alone without cargoes were investigated using calcein leakage experiments in zwitterionic POPC and 30% negatively charged (POPC/POPG) LUVs. In the absence of peptides (or peptide/cargo complexes), no leakage of calcein from the LUVs was observed. The fluorescence intensity in this case was low and stable due to the self-quenching of concentrated calcein inside the LUVs and low permeability of the phospholipid vesicle membrane to the calcein molecules. After the addition of the peptides to LUVs, the entrapped calcein could be released into the buffer outside the LUVs as a result of peptide-induced leakage, leading to an increase in fluorescence intensity. CPPs were added to the calcein-entrapping LUV solution which either consisted of 100 μM POPC or 100 μM POPC/POPG (7:3) and the calcein release was recorded at various time points at 20 °C. In each titration, fluorescence intensity was recorded during 10 min incubation. Fig. 1A shows the time-dependence of calcein leakage from 30% negatively charged LUVs induced by NF1 (8 μM). Fluorescence was recorded immediately after addition of the peptide followed by 2 min intervals until the signal was maintained constant. The profiles were similar for all peptides indicating that the process is a relaxation towards equilibrium and has a duration of approximately 10 min. This observation has been discussed in terms of transient pore formation, which may stabilize the spontaneous leakage [45]. Fig. 1B shows the percent of leakage induced by TP10 and its derivatives at different peptide-to-lipid molar ratios with neutral POPC LUVs and (C) with 30% negatively charged POPC/POPG LUVs, after 10 min of incubation at 20 °C. Based on Fig. 1A, the leakage values shown in Fig. 1B and C should represent the final level at each peptide concentration. A clear difference between peptides regarding their induction of calcein leakage from LUVs was observed for both neutral and partially negatively charged LUVs. As shown in Fig. 1B and C, we observed a significant calcein release for NF51 at quite low concentrations, comparable with its parent peptide TP10. However, the membrane perturbation and the percent of leakage for PF3 and NF1 were weaker and the peptide concentration had therefore to be increased in order to induce clearly detectable leakage. Interestingly, lower peptide–membrane perturbation from the treatments was observed for all CPPs examined with 30% negatively charged LUVs compared to neutral POPC LUVs. Table 2

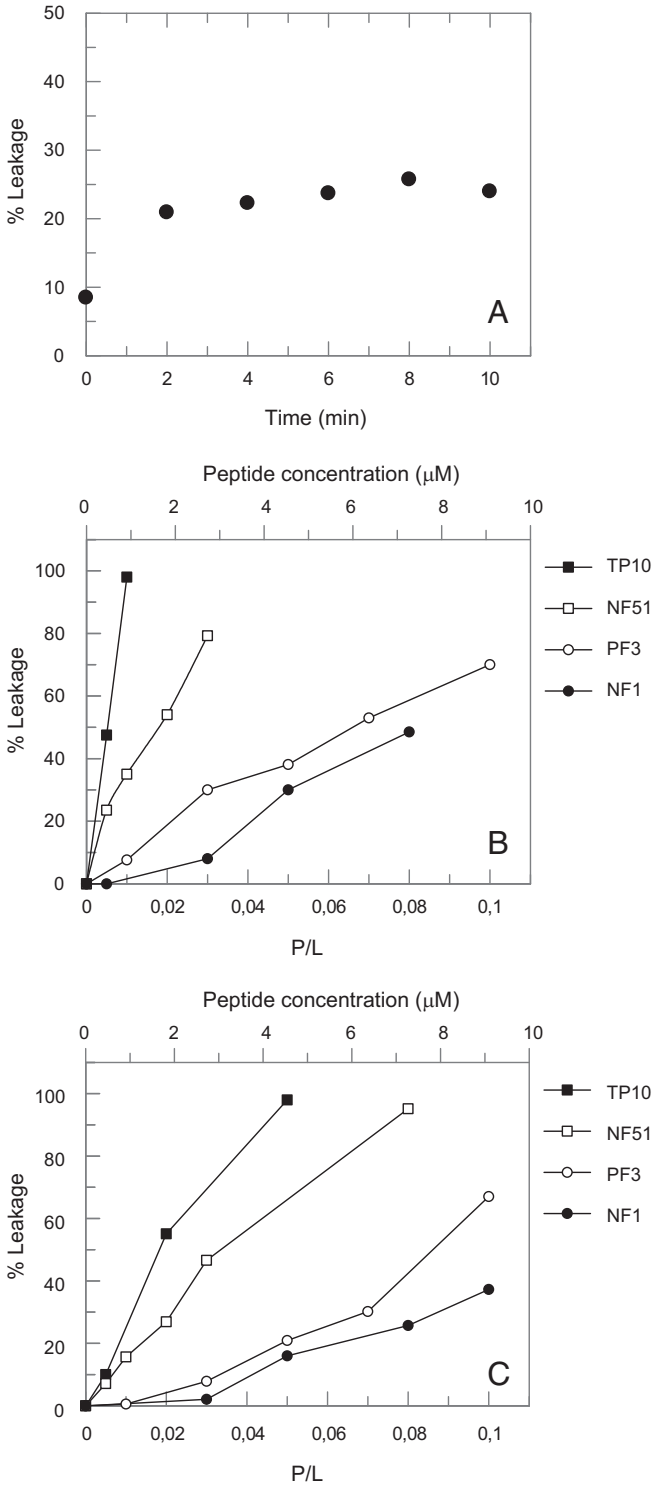

Fig. 1. A) Time-dependence of calcein release due to addition of 8 μM NF1 to a vesicle solution containing 55 mM entrapped calcein inside 100 μM negatively charged POPC/POPG (7:3) LUVs at 20 °C. The percent of calcein leakage was measured for 10 min immediately after addition of the peptide, and plotted as a function of time (min). The medium was 50 mM phosphate buffer (pH 7.4). Calcein leakage experiment with TP10 and the three derivatives, PF3, NF1 and NF51, titrated to a vesicle solution containing 55 mM entrapped calcein inside B) 100 μM zwitterionic POPC LUVs and C) 100 μM negatively charged POPC/POPG (7:3) LUVs at 20 °C. The percent of calcein leakage was measured 10 min after adding different amounts of the peptides, and plotted as a function of total peptide-to-lipid molar ratio, P/L. The medium was 50 mM phosphate buffer (pH 7.4).

summarizes the leakage values which are normalized to the values for PF3 (without cargo) and corrected for peptide concentrations.

3.2. Characteristics of peptide/cargo complex: surface charge and size measurements

To understand the contribution of the surface charges in membrane perturbation effects of CPPs and CPP/cargo complexes, the surface charge state of peptides and peptide/cargo complexes were characterized using a zeta-potential analyzer. The complex was based on an oligonucleotide (pGL3, SCO or siRNA) mixed with the peptide at an optimal peptide concentration (Table 1) in water and co-incubated for 30 min. This resulted in spontaneous formation of a non-covalent conjugate between the cargo and the peptide [46]. We have measured the zeta-potential in water that mimics the properties of the complexes before addition to the vesicle solution. After addition, both buffer solution and vesicles may affect the surface charge density. Zeta-potentials of NickFect peptides were previously measured in physiological conditions [26,27]. Table 2 shows the zeta-potential measured for the peptide/cargo molecules in water.

Complexes with zeta-potential values which are higher than +30 mV or lower than −30 mV are considered stable [47–49]. While all investigated cargoes have negative zeta-potentials in water (data not shown), the zeta value of all CPP/pGL3 complexes in water was positive at a charge ratio of 3. Plasmid together with TP10 formed a less stable particle with a zeta value of +11.1 ± 3.7 mV compared to other CPP/pGL3 complexes having a larger value than +30. Similar to plasmid complexes, the CPP/SCO complexes formed at molar ratios of 10 were largely positively charged. The zeta-potential values of some CPP/siRNA complexes were dramatically changed at molar ratio 20. NF1/siRNA and NF51/siRNA complexes had zeta values of −51.8 ± 2.52 and +17.5 ± 1.42 mV, respectively. However, CPP/siRNA complexes with TP10 and PF3 were largely positively charged at this molar ratio (Table 2). All free peptides except TP10 showed highly positive zeta-potentials in water indicating the presence of stable particles having positive surface charge (data not shown).

DLS was used in order to measure the size of the partially negatively charged vesicles. Effects of NF51, NF1 and PF3 as well as impact of peptide/cargo complexes on the vesicle size and homogeneity were also investigated. The size of the vesicle was approximately 100 nm in diameter and addition of NF51 slightly increased the vesicle diameter. Both NF51/SCO and NF51/siRNA complexes increased the size of the vesicles and resulted in broader peaks. Interestingly, NF51/pGL3 complexes induced three different populations (Fig. S1–4). Similar effects were observed for the other investigated peptides (data not shown).

3.3. Interaction of peptide/cargo complex with the model membrane

To determine the impact of incorporation of the cargo molecules into the CPPs on the interaction with the phospholipid membrane, the calcein leakage experiment was performed with both uncharged and partially negatively charged vesicles. The experiments were performed by addition of the peptide/cargo complex to the calcein-entrapping LUVs and recording the calcein fluorescence intensity for 10 min as previously done with the peptides alone.

Fig. 2 shows the effect of different cargoes on peptide–membrane perturbation and leakage with uncharged (A) and 30% negatively charged (B) LUVs. Similar effects were observed for NF1 and NF51 in complex with the cargoes. For both peptides, a drastic decrease in the membrane leakage could be seen when they were in complex with pGL3 compared to the peptide alone. Indeed, there was relatively lower effect of SCO on membrane leakage for NF1 and NF51. siRNA also decreased the amount of leakage and had a stronger reduction effect on membrane perturbation caused by NF51. Membrane charge had a small effect on peptide/cargo membrane perturbation for NickFect peptides. PF3 acted differently in a way that the added cargo

Table 2
Summary of CPP-mediated uptake and peptide interaction with POPC and POPC/POPG (7:3) LUVs, in the absence and presence of the cargo.

CPP		TP10	PF3	NF1	NF51
Relative cellular uptake[2]	No cargo	n.d.[1]	1	0.9	0.5
After 15 min	CPP/pGL3	n.d.	0.9	0.03	0.025
Peptide: 0.5 μM	CR3				
	CPP/SCO	n.d.	0.6	0.17	0.78
	MR10				
	CPP/siRNA	n.d.	0.4	0.8	0.99
	MR20				
Relative cellular uptake[2]	No cargo	n.d.	1	0.97	0.77
After 30 min	CPP/pGL3	n.d.	0.99	0.05	0.07
Peptide: 0.5 μM	CR3				
	CPP/SCO	n.d.	0.6	0.3	0.7
	MR10				
	CPP/siRNA	n.d.	0.9	0.8	0.95
	MR20				
Relative cellular	No cargo	n.d.	1	0.98	0.97
uptake[2]	CPP/pGL3	n.d.	1	0.1	0.2
After 60 min	CR3				
Peptide: 0.5 μM	CPP/SCO	n.d.	0.95	0.5	0.95
	MR10				
	CPP/siRNA	n.d.	1	0.98	0.97
	MR20				
POPC	No Cargo	n.d.	1	0.8	3.5
Relative membrane perturbation[3]	CPP/pGL3	n.d.	1.1	0	0
	CR3				
	CPP/SCO	n.d.	1.7	0.5	2.4
	MR10				
	CPP/siRNA	n.d.	0.8	0.2	0
	MR20				
POPC/POPG (7:3)	No Cargo	n.d.	1	0.8	3.2
Relative membrane perturbation[3]	CPP/pGL3	n.d.	0.9	0	0.3
	CR3				
	CPP/SCO	n.d.	0.8	0.5	1.6
	MR10				
	CPP/siRNA	n.d.	0	0.4	0.1
	MR20				
Zeta-potential	CPP/pGL3	11.1 (3.7)	61.2 (5.1)	35.1 (0.71)	46.5 (1.96)
(in water)[4]	CR3				
(mV)	CPP/SCO	11.5 (3.81)	45.2 (1.57)	38.1 (1.94)	39.8 (3.32)
	MR10				
	CPP/siRNA	3.65 (1.13)	34.8 (1.69)	−51.8 (2.52)	17.5 (1.42)
	MR20				

[1] Not determined.
[2] The cellular uptake values are normalized to values for PF3 without cargo.
[3] For comparison, leakage values are normalized to values for PF3 (without cargo) and corrected for peptide concentrations.
[4] For zeta-potential, the value in the parenthesis is standard deviation.

has different effects on membrane perturbation caused by the peptide compared to NickFect peptides. Interestingly, there is almost no effect of plasmid on PF3–membrane interaction and leakage, independent of the membrane charge. However, membrane charge altered the effects of SCO and siRNA on membrane perturbation caused by PF3. With charged vesicles, siRNA inhibited the leakage caused by PF3 and the addition of SCO had no clear effect on PF3 membrane leakage. In contrast, the effects were opposite with uncharged vesicles (Table 2). As a control experiment, cargoes alone were added to the vesicles. In the absence of peptides, no leakage of calcein from the LUVs was observed (data not shown).

3.4. Induction of secondary structure by peptide and peptide/cargo complex

TP10 derivative peptides and their possible structure induction in buffer and in the presence bio-membrane mimicking systems were studied by CD spectroscopy. The temperature was 20 °C in all measurements. Similar to leakage experiments, the peptide concentration was chosen in which optimal membrane perturbation could be observed (Table 1). Both buffer and vesicle solution were used as blank samples and baseline correction was used for the blank. Fig. 3A and B show the CD spectra of peptides in the buffer, and in the presence of uncharged vesicles, respectively. All stearylated peptides adopted an alpha helical structure in aqueous buffer. Indeed, CD spectroscopy revealed no dominating secondary structure component for TP10 in buffer. In the 100 μM vesicle solution, with either charged or uncharged membrane, similar helical structures were induced in stearylated peptides, with slightly higher intensity in negatively charged vesicles (Fig. S5). However, TP10 showed different structures with vesicles depending on the membrane charge. TP10 in vesicle solution containing negatively charged membrane adopted an alpha helix structure and it is overall more structured compared to the structure formed with uncharged vesicles. With uncharged vesicles, TP10 showed a structure similar to that in the buffer. Taking into account the intensity of the peak at 222 nm, it is clear that the helicity in the stearylated peptides is weaker compared to TP10 with negatively charged LUVs.

We studied the impact of the presence of SCO and plasmid on peptide secondary structure in the presence of vesicles with uncharged and 30% negatively charged membranes. In order to clearly observe the influence of different cargoes, the spectra of the peptide alone and peptide with the cargo were plotted in the same graph. With uncharged LUVs, the CD spectra of PF3/SCO (Fig. 4A) and NF1/SCO (Fig. S6) were not affected by the presence of SCO. The CD spectra were characterized by two minima at 208 and 222 nm indicating an alpha helical state. However, SCO changed the NF51 secondary structure in uncharged vesicles (Fig. 4B). The CD spectra of peptides were not affected by the presence of SCO in 30% negatively charged vesicles (data not shown). Poor structure induction can be seen when plasmid is in complex

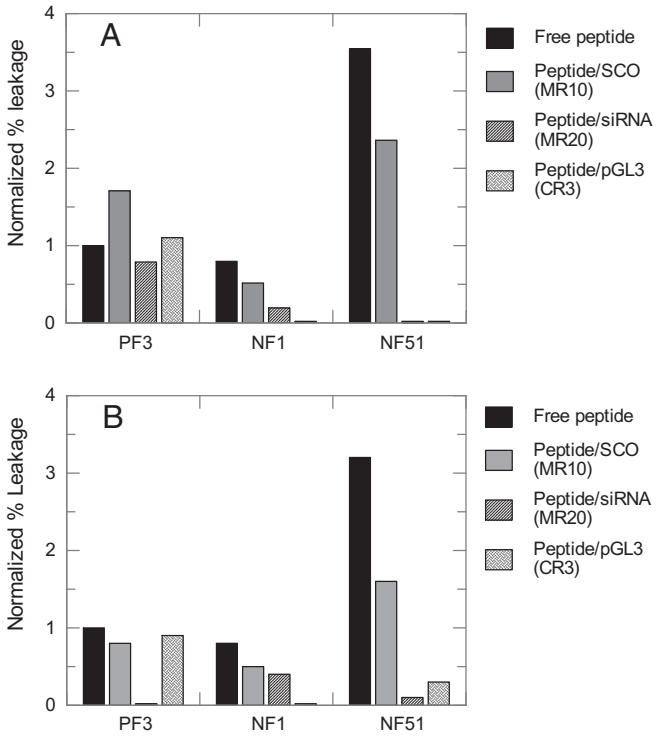

Fig. 2. Calcein leakage due to addition of the peptides in the presence of oligonucleotide cargoes (SCO, siRNA and pGL3) to a vesicle solution containing 55 mM entrapped calcein inside A) 100 μM zwitterionic POPC LUVs and B) 100 μM negatively charged POPC/POPG (7:3) LUVs at 20 °C. The percent of calcein leakage was measured 10 min after adding different peptides and peptide/cargo complexes. The medium was 50 mM phosphate buffer (pH 7.4). All peptide/cargo complexes were prepared using an optimal peptide concentration, i.e. a concentration that results in an observable percentage of calcein leakage (2 μM for NF51, 5 μM for PF3 and 8 μM for NF1). Ratios between peptide and cargo are based on previously determined optimal ratios for efficient cellular transfection assays [4,26,27]. The leakage values were normalized to values for PF3 (without cargo) and corrected for peptide concentrations.

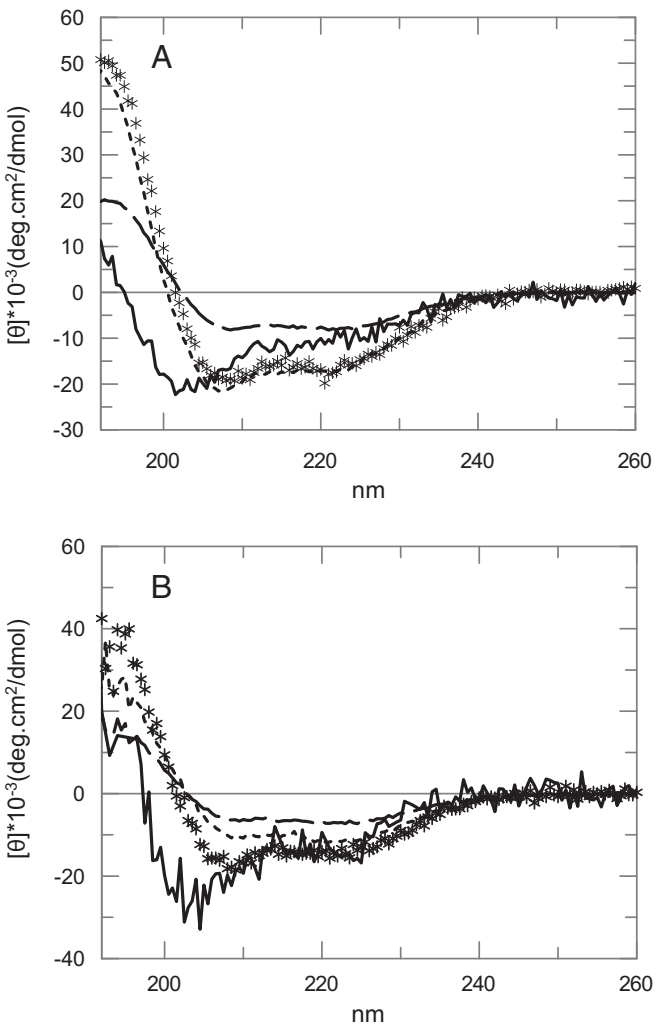

Fig. 3. CD spectra of TP10 (solid line), PF3 (dots), NF1 (dashed line) and NF51 (stars) in A) 10 mM potassium phosphate buffer and B) in 100 μM zwitterionic POPC LUVs, pH 7.4 at 20 °C. Spectra were corrected by subtracting the buffer (or the LUVs) as a background.

with the peptide, independent on the membrane charge (Figs. 4A, B and S6).

3.5. Cellular uptake efficiency of fluorescently labeled peptides

To evaluate the efficiency of the peptide internalization, FACS analysis of HeLa cells exposed to FAM-labeled PF3, NF1 and NF51 was performed. The cells were treated for 15, 30 and 60 min with peptides at different concentrations (0.5–5 μM). Fig. 5 shows the number of the cells that has taken up the peptides relative to the untreated cells at different concentrations. The FAM-labeled peptides were able to cross the cellular membrane of HeLa cells as investigated by FACS analysis (Table 2). The results revealed that the number of cells containing the peptide depends on the incubation time and the peptide concentration and that this dependency was more dominant for NF51. The extent of cellular uptake of NF1 and PF3 was significantly higher than that observed for NF51 after 15 min incubation. NF51 at higher concentrations of 2 and 3.5 μM showed similar high uptake efficiency as the other examined peptides while at 0.5 μM NF51 required more incubation time to transfect the whole cell population (Fig. 5).

3.6. Effect of cargoes on cellular uptake efficiency

To investigate the impact of the cargoes on peptide-cellular uptake efficiency, we carried out experiments where preformed peptide/cargo complexes were incubated with the cells in the same way as we did for free peptides. To establish non-covalent complexes of the peptides with different cargoes, we used the same peptide/cargo ratios that we have used for leakage experiments (Table 1).

In the presence of cargo molecules, the cellular uptake was changed for most peptide/cargo complexes depending on the type of the cargo, type of the peptide and peptide concentration (Fig. 6A and B). PF3/pGL3 showed to be taken up equally well as the free PF3. However, the uptake of NF1 and NF51 in complex with pGL3 was dominantly diminished after 15 min of incubation and this effect was more pronounced at lower peptide concentrations (Fig. 6A). Increasing concentrations of added peptide/cargo complexes restored the uptake efficiency for NF51 nearly to the level of free NF51 uptake. For NF1 even at higher concentrations only 60% from the uptake level of the free peptide was achieved with NF1/pGL3 complexes (Fig. 6B).

With siRNA the cellular uptake was decreased for PF3 complex, while complex formation with siRNA had no impact to NF51 and NF1 cellular internalization (Fig. 6A). Furthermore, for the PF3/siRNA complex, the internalization level reached that of the free peptide at higher concentrations (Fig. 6B). The complexes of all the peptides with SCO entered HeLa cells at lower speed and amount than free PF3. At higher concentrations of the NF51 and PF3 complexes internalization level reached the level of free PF3, while NF1/SCO complexes reached about 80% of that level (Fig. 6B).

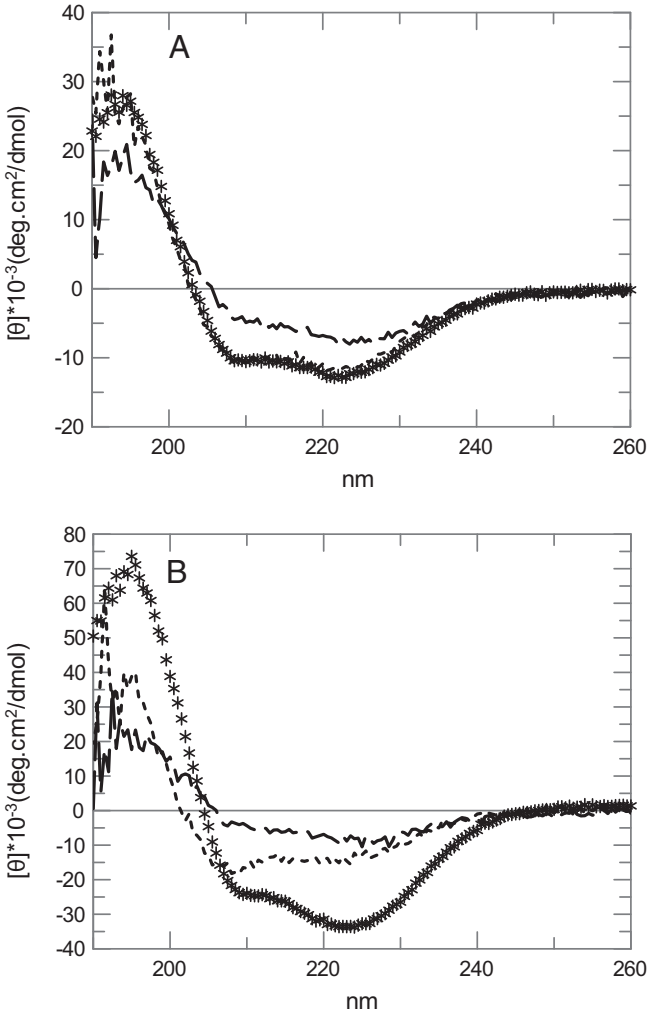

Fig. 4. Effect of cargoes on the CD spectra of peptides. A) CD spectra of PF3/SCO, MR10 (stars) and PF3/pGL3, CR3 (dashed line) in 100 μM zwitterionic POPC LUVs compared to CD spectra of PF3 in 100 μM zwitterionic POPC LUVs (dots), B) CD spectra of NF51/SCO, MR10 (stars) and NF51/pGL3, CR3 in 100 μM zwitterionic POPC LUVs (dashed line) compared to CD spectra of NF51 in 100 μM zwitterionic POPC LUVs (dots). Spectra were recorded at 20 °C and they are corrected by subtracting the buffer (or LUVs) as a background.

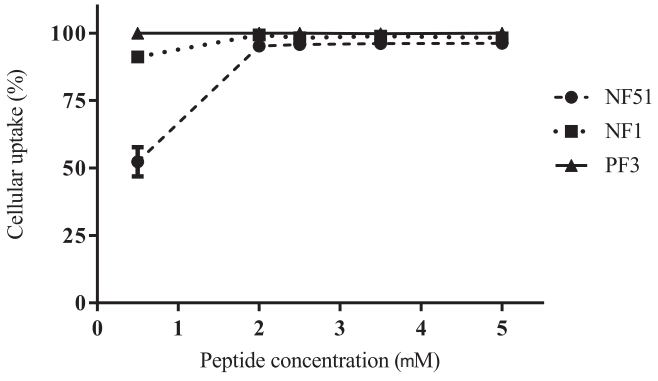

Fig. 5. Cellular uptake of FAM-labeled PF3, NF1 and NF51 in HeLa cells in serum containing medium. HeLa cells were incubated with increasing concentrations of peptides for 15 min at 37 °C and transfected cell population was evaluated by FACS analysis. The results were presented as percentage to live cells.

3.7. Delivery of bioactive oligonucleotides

Functional assays were also performed to observe biological responses as well as to evaluate the endosomal escape efficiency of the peptide/cargo complex. We have used three biological activity experiments including a splice-switching assay representing a positive read-out based on the presence of the SCO in the nucleus and correcting the aberrant splice site [50], a siRNA down-regulation assay which is a negative read-out considering the delivery of the siRNA to the cytoplasm to induce the gene silencing effect [51] and finally a plasmid transfection assay based on using a luciferase-encoding plasmid (pGL3) and measuring the luciferase activity [52].

For pGL3, NF51 mediated about 2 fold higher transfection level compared to NF1. Still, gene expression levels achieved both by NF51 and NF1 exceeded the luciferase level reached with PF3 about 1000 fold (Fig. S8). In the splice-switching assay NF1 induced the highest amount of SCO intracellular delivery, reaching 1.5–2 times higher splice correction levels than NF51 and 3–4 times higher than PF3 (Fig. S7). The maximal gene silencing was achieved with NF51/siRNA complexes resulting in 90% knock-down of luc-gene. NF1/siRNA and PF3/siRNA complexes mediated target gene down-regulation was less efficient, reaching 60% and 30% knock-down, respectively (Fig. 7).

4. Discussion

In the present work, we have used the calcein leakage experiment to characterize the membrane perturbation effects of three different CPPs in the absence and presence of different cargo molecules. They are all TP10 based N-terminally stearylated peptides and they slightly differ regarding amino acid residue composition and chemical structure. We already knew that TP10 is very potent to disturb model membranes at low concentrations and that its stearylated version, PF3 shows increased amphipathicity and improved insertion but decreased leakage and hence lower membrane perturbation capacity into a lipid monolayer composed of zwitterionic lipids [25]. Due to their similar characteristics, TP10 and PF3 were used as control peptides to study two new stearylated TP10 analogs, NF1 and NF51. In addition, we studied the cellular uptake efficiencies of these peptides in the absence and presence of the cargo molecules and compared their biological activities. Our results may clarify the mechanistic parameters essential for the endosomal escape when a cargo is attached to the CPP.

Peptides that perturb the phospholipid membrane or cause membrane leakage are often discussed in terms of a balance between average hydrophobicity and total positive charges. Comparing stearylated TP10 analogs (Table 1), we observed that they vary in the context of average hydrophobicity as well as the total positive charge. Interestingly, a clear difference in calcein release was also observed with both neutral and partially negatively charged LUVs treated with TP10 modified peptides (Fig. 1B and C). The two CPPs, PF3 and NF1, behave similarly, giving rise to substantial leakage of the vesicle contents, but NF1 which is the most hydrophilic between the studied peptides, required a higher concentration to perturb the membrane and cause calcein to leak out. Additionally, NF1 has one negatively charged phosphate group that may decrease its interaction with the membrane due to the electrostatic repulsion. The highest degree of leakage was observed for NF51, the most hydrophobic peptide, which was potent already at a low concentration of 2 μM. In a recently published study, NF51 and NF1 showed different endosomolytic properties and endosomal escape was the main problem for NF1 in gene transfection. It is shown that NF51/pGL3 can quickly redistribute from early endosomes to the cytoplasm [28]. Endosomal escape is also relatively limited for PF3 [4]. We suggest that peptide hydrophobicity as well as peptide chemical structure is the driving force in membrane perturbation and leakage. Moreover, presence of ornithine in NF51 may have an additional effect on model membrane interactions. Our results indicate a correlation between phospholipid membrane perturbation and endosomal escape efficiencies of investigated CPPs. NF51

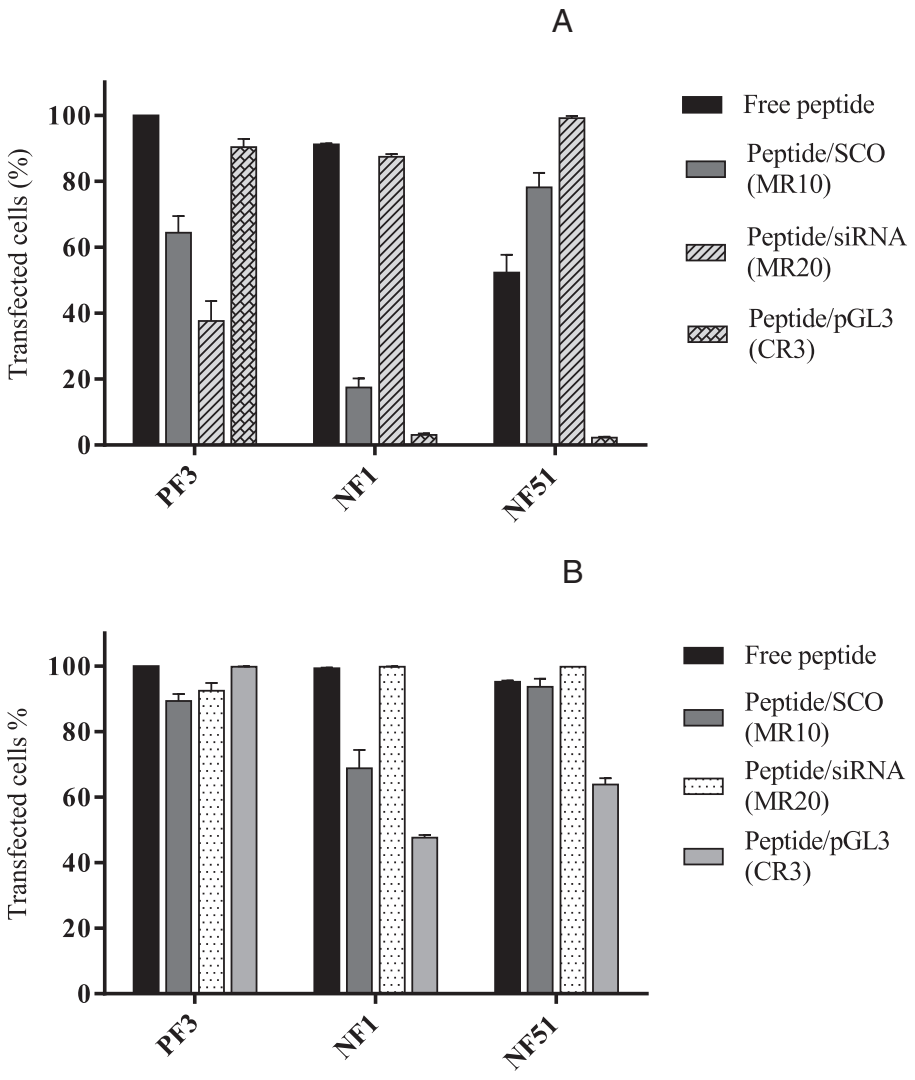

Fig. 6. Effect of cargoes on cellular uptake efficiency of FAM-labeled PF3, NF1 and NF51 in HeLa cells in serum containing media. Complexes of FAM-labeled peptides with different cargoes were preformed at A) 0.5 μM and B) 2 μM peptide concentrations. Cargo concentration was calculated according to peptide concentration using charge ratio 3 for pGL3, molar ratio 10 for SCO and molar ratio 20 for siRNA. Transfected cell population was evaluated by FACS analysis 15 min after transfection at 37 °C and presented as percentage to live cells.

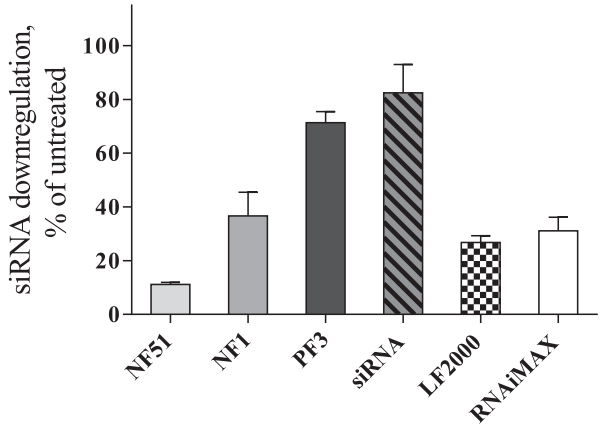

Fig. 7. Inhibition of luciferase expression using peptide/siRNA complexes. HeLa cells were transfected with BES PX plasmid, containing luc2 gene 24 h before treatment with preformed NF1, NF51 and PF3 complexes with siRNA MR 20 (final concentration 100 nM siRNA) in serum containing medium. Luciferase activity was measured 24 h after transfection. Untreated cells were taken as 100%. Free siRNA was utilized as a negative control and Lipofectamine 2000 and LF RNA iMAX as positive controls.

with the ability to perturb the model membrane at quite low concentrations is efficient in endosomal escape. Analyzing FACS results showed that NF51 has about 2-fold lower cellular uptake efficiency compared to NF1 and PF3 (Fig. 5 and Table 2). This observation further suggests the presence of different mechanisms in peptide cellular internalization and endosomal escape. NF51 has strong ability to perturb the endosomal membrane while utilizing a slower internalization mechanism compared to NF1 and PF3. From the treatments with partially negatively charged LUVs, a slightly lower peptide membrane perturbation compared to uncharged LUVs for all CPPs examined (Fig. 1C) can be observed. Negatively charged vesicles might create a strong interaction with the positively charged peptides, keeping peptides at the vesicle membrane surface and not allowing them to penetrate more deeply into the membrane. Alternatively, it is due to the different vesicle–membrane permeability caused by charged or uncharged phospholipids. We also showed that decreasing the pH outside the LUVs from 7.4 to 5 enhanced the NF1 membrane perturbation and leakage and this effect was dominant for NF1 compared to the other investigated peptides (data not shown). A simple explanation is that NF1 has a pH sensitive group that destabilizes the vesicle membrane in the acidic environment.

Another interesting question was whether the CPP follows the same membrane perturbation efficiency when electrostatically attached to a

cargo. With pGL3, the two NickFect peptides exhibited very similar behavior in terms of membrane interactions. An almost complete inhibition of leakage was observed for NF1/pGL3 and NF51/pGL3 independent of membrane charge (Fig. 2A and B). This can be related to the formation of stable and large complexes between peptide and pGL3 and once the peptide is captured in the complexes it is not available to interact efficiently with the membrane and induce perturbation. The stability of NickFect/pGL3 complexes was previously studied through heparin displacement assay where both peptides showed resistance to treatment with heparin [28]. Both DLS measurements (Fig. S2) and zeta-potential values (Table 2) for NF51/pGL3 confirm this hypothesis. In the case of PF3, the presence of pGL3 had no effect on the degree of interaction and perturbation with both uncharged and partially charged LUVs.

The result suggests that PF3 may condense pDNA differently from NickFect peptides resulting in different interactions. In agreement with leakage studies, cellular uptake experiments using FACS showed that pGL3 has no effect on PF3 uptake however it largely decreases NickFect cellular uptake efficiencies at 0.5 μM after a 15 min treatment (Fig. 6A). In the pGL3 transfection assay, PF3 shows a smaller enhancement of pGL3 delivery even though the PF3/pGL3 is being rather efficiently internalized. Leakage experiments as performed here may not completely reflect the behavior of the NickFect/pGL3 complexes in the endosomes, because the complexes may be stable in the buffer used for the calcein experiments but may partially dissociate in endosomes. Low pH inside the endosome may destabilize the complex and produce more free peptides with more tendencies to leak out from the endosome. We should also observe that NF1 is a pH sensitive peptide containing a functional group with buffering capacity which acts differently when pH drops inside the endosomes causing more membrane perturbation. Based on these observations together with high pGL3 transfection efficiencies of NickFects (Fig. 7), we may conclude that the rate limiting step for NickFect/pGL3 cellular transfection is the cellular internalization and not endosomal escape. Once the complex is inside the endosome, free NickFect peptides destabilize the endosomal membrane and promote the endosomal escape. In contrast, the translocation of the PF3/pGL3 through the endosomal membrane is the rate limiting step for PF3 bioactivity due to the less membrane disruptive effect of PF3.

Small effects on the membrane perturbation and leakage were obtained for the peptide/SCO complexes (Fig. 2A and B). The fact that the SCO cargo is a small molecule might leave the peptides in the complex exposed to the environment, thus they are still able to interact with the membrane and cause leakage. The DLS measurement also showed one population with slightly larger size when SCO complexes interact with the vesicles (Fig. S3). SCO enhanced the cellular uptake efficiency of NF51. This observation indicates the positive effect of SCO on membrane permeation for NF51, and could possibly facilitate internalization of NF51 associated SCO molecules by changing the uptake mechanism. Similar to plasmid transfection assay, NickFects show higher splice-correcting activity compared to PF3.

In leakage experiments, siRNA shows distinct effects depending on the peptide and membrane charge (Fig. 2A and B). With 30% negatively charged LUVs, siRNA complexes almost completely inhibited the membrane perturbation of PF3 however the effect on NF1 potency was not that strong (Fig. 2B). In contrast, with uncharged LUVs, complete leakage inhibition was observed for NickFects in complex with siRNA (Fig. 2A). These observations suggest that electrostatic interactions may have an important role in peptide/siRNA membrane interactions due to the structural characteristics of siRNA complexes.

CD spectra of peptides in buffer (Fig. 3A) clearly show that the secondary structure of TP10 changes in its derivatives. TP10 adopted mainly a random coil structure while all stearylated TP10 based peptides showed an alpha helical structure in the buffer. This structural difference is due to the hydrophobic nature of stearylated N-terminus that drive the peptide to adopt a helical conformation, possibly by forming micelle-like particles. Neither secondary structures nor the amount of membrane leakage of stearylated peptides was strongly dependent on the choice of vesicle membrane charge.

Secondary structural induction of stearylated peptides in the presence of vesicles were also investigated when they were in complex with cargoes, SCO and pGL3 (Fig. 4A and B). The structure changed only slightly for SCO complexes with PF3 and NF1 in the presence of LUVs independent of membrane charge. This clearly indicates that the peptide secondary structure is not affected by the presence of SCO, or that most peptides are exposed to the vesicle membrane and keep their conformation. However, the NF51 secondary structure changed when it was in complex with SCO in the presence of uncharged LUVs. Results for all investigated peptide/pGL3 complexes were different showing a relatively weak helical structure with both charged and uncharged vesicles. This may be explained by an equilibrium between an unstructured peptide in complex with the cargo and some free peptides that are structured. Both CD results with SCO and pGL3 are in agreement with leakage results showing that SCO has less effect on the peptide–membrane perturbation compared to pGL3. The weaker influence of SCO compared to pGL3 on peptide secondary structure as well as leakage could be due to differences in the chemical structure of the complex, possibly combined with a higher presence of free peptides for the SCO complex.

It should also be observed that NF1 appears to be most efficient for cargo delivery into the nucleus where SCO has its function, while NF51 is the most efficient for both cytoplasmic and nucleus delivery where siRNA and pDNA are functional, respectively. The fact that NF51 changes its secondary structure in complex with SCO (Fig. 4B) may be related to its less efficiency SCO delivery. It also raises the question of how complex stability contributes to the functionality of the different complexes.

In summary, the rate-limiting step for NF1 and NF51 in the three performed biological assays should therefore be cellular membrane perturbation and internalization. The hydrophobicity of an efficient peptide should therefore be an important parameter in endosomal membrane interaction and endosomal escape. However, the electrostatic interaction between the cellular membrane and the peptide/cargo complex may promote different mechanisms of cellular uptake. Whereas the proteoglycans would possibly interact with positively charged particles [53] and negatively charged particles preferentially interact with scavenger receptors [54]. Each type of complex could thus have its particular entry pathway. In this context, it should also be pointed out that our results do not rule out the participation of a CPP uptake mechanism involving plasma membrane destabilization.

As shown in Figs. 1 and 2, the biophysical properties of NF51 and its siRNA complex show that peptide alone causes strong membrane leakage while the cargo complex does not induce leakage. In addition, the complex stability and its capacity to partially dissociate inside the endosome may play an important role on the biological activity of an efficient peptide vector. This may be the biophysical signature of an efficient delivery vector.

5. Conclusions

Our results show that the most hydrophobic peptide, NF51 in this work, has the highest membrane perturbing effect. Equally important, the chemical structure of a peptide may enhance its membrane interaction. While there is no obvious correlation between cellular uptake and endosomal escape efficiencies, results with membrane leakage caused by NickFects are in good agreement with the endosomal escape efficiency of the peptide. The present study also indicates different degrees of membrane leakage and cellular uptake efficiency for peptides electrostatically attached to cargo compared to free peptides. For NickFect peptides, membrane perturbation was reduced in the presence of cargoes and this effect was much more pronounced for a large cargo like pGL3. Based on our results, cellular internalization is the rate limiting step

for NickFects in complex with the cargo. The present results lead to two main conclusions: 1) The peptide and its physico-chemical properties, mainly its hydrophobicity and chemical structure define its membrane perturbation efficiency and thus its ability to escape from the endosomes; 2) peptide complexes have different cellular uptake efficiencies which are cargo type dependent but independent of the endosomal escape. Our work shows a complete and directed study addressing the influence of the most significant oligonucleotide therapeutic cargo in cell–penetrating peptide interaction with cellular membranes. These findings may also have implication on the development of new TP10-based modified CPPs that will have favorable properties leading to even more efficient transport vector for intracellular delivery of nucleic acids and gene therapy.

Acknowledgments

This work was supported by the Swedish Research Council (VR-NT), the Swedish Cancer Foundation, the Innovative Medicines Initiative Joint Undertaking under grant agreement no. 115363; resources of which are composed of financial contribution from the European Union's Seventh Framework Programme (FP7/2007-2013) (IMI) and EFPIA companies in kind contribution, targeted financing project IUT20–26 from the Estonian Ministry of Education and Research, Estonian Science Foundation grant ETF9438 and by the EU through the European Regional Development Fund through the Centre of Excellence in Chemical Biology.

Appendix A. Supplementary data

Supplementary data to this article can be found online at http://dx.doi.org/10.1016/j.bbamem.2014.08.011.

References

[1] S.L. Lo, S. Wang, An endosomolytic Tat peptide produced by incorporation of histidine and cysteine residues as a nonviral vector for DNA transfection, Biomaterials 29 (2008) 2408–2414.
[2] T. Lehto, K. Ezzat, Ü. Langel, Peptide nanoparticles for oligonucleotide delivery, Prog. Mol. Biol. Transl. Sci. 104 (2011) 397–426.
[3] Y. Wolf, S. Pritz, S. Abes, et al., Structural requirements for cellular uptake and antisense activity of peptide nucleic acids conjugated with various peptides, Biochemistry 45 (2006) 14944–14954.
[4] M. Mäe, S. El Andaloussi, P. Lundin, et al., A stearylated CPP for delivery of splice correcting oligonucleotides using a non-covalent co-incubation strategy, J. Control. Release 134 (2009) 221–227.
[5] A. Eguchi, B.R. Meade, Y.C. Chang, et al., Efficient siRNA delivery into primary cells by a peptide transduction domain-dsRNA binding domain fusion protein, Nat. Biotechnol. 27 (2009) 567–571.
[6] S.E. Andaloussi, T. Lehto, I. Mäger, et al., Design of a peptide-based vector, PepFect6, for efficient delivery of siRNA in cell culture and systemically in vivo, Nucleic Acids Res. 39 (2011) 3972–3987.
[7] L. Vasconcelos, K. Pärn, Ü. Langel, Therapeutic potential of cell-penetrating peptides, Ther. Deliv. 4 (2013) 573–591.
[8] A. Mitsueda, Y. Shimatani, M. Ito, et al., Development of a novel nanoparticle by dual modification with the pluripotential cell-penetrating peptide PepFect6 for cellular uptake, endosomal escape, and decondensation of an siRNA core complex, Biopolymers 100 (2013) 698–704.
[9] A.H. van Asbeck, A. Beyerle, H. McNeill, et al., Molecular parameters of siRNA–cell penetrating peptide nanocomplexes for efficient cellular delivery, ACS Nano 7 (2013) 3797–3807.
[10] S. Lindberg, A. Muñoz-Alarcón, H. Helmfors, et al., PepFect15, a novel endosomolytic cell-penetrating peptide for oligonucleotide delivery via scavenger receptors, Int. J. Pharm. 441 (2013) 242–247.
[11] A. Ziegler, Thermodynamic studies and binding mechanisms of cell-penetrating peptides with lipids and glycosaminoglycans, Adv. Drug Deliv. Rev. 60 (2008) 580–597.
[12] F. Madani, S. Lindberg, Ü. Langel, et al., Mechanisms of cellular uptake of cell-penetrating peptides, J. Biophys. 2011 (2011) 1–10.
[13] F. Said Hassane, A.F. Saleh, R. Abes, et al., Cell penetrating peptides: overview and applications to the delivery of oligonucleotides, Cell. Mol. Life Sci. 67 (2010) 715–726.
[14] F. Duchardt, M. Fotin-Mleczek, H. Schwarz, et al., A comprehensive model for the cellular uptake of cationic cell-penetrating peptides, Traffic 8 (2007) 848–866.
[15] F. Madani, A. Perálvarez-Marín, A. Gräslund, Liposome model systems to study the endosomal escape of cell-penetrating peptides: transport across phospholipid membranes induced by a proton gradient, J. Drug Del. 2011 (2011) 1–7.
[16] F. Madani, R. Abdo, S. Lindberg, et al., Modeling the endosomal escape of cell-penetrating peptides using a transmembrane pH gradient, BBA-Biomembr. 1828 (2013) 1198–1204.
[17] J.S. Wadia, R.V. Stan, S.F. Dowdy, Transducible TAT-HA fusogenic peptide enhances escape of TAT-fusion proteins after lipid raft macropinocytosis, Nat. Med. 10 (2004) 310–315.
[18] A. El-Sayed, S. Futaki, H. Harashima, Delivery of macromolecules using arginine-rich cell-penetrating peptides: ways to overcome endosomal entrapment, AAPS J. 11 (2009) 13–22.
[19] T. Endoh, T. Ohtsuki, Cellular siRNA delivery using cell-penetrating peptides modified for endosomal escape, Adv. Drug Deliv. Rev. 61 (2009) 704–709.
[20] M. Pooga, M. Hällbrink, M. Zorko, Ü. Langel, Cell penetration by transportan, FASEB J. 12 (1998) 67–77.
[21] U. Soomets, M. Lindgren, X. Gallet, et al., Deletion analogues of transportan, BBA-Biomembr. 1467 (2000) 165–176.
[22] K. Kilk, Ü. Langel, Cellular delivery of peptide nucleic acid by cell-penetrating peptides, Methods Mol. Biol. 298 (2005) 131–141.
[23] P. Guterstam, F. Madani, H. Hirose, et al., Elucidating cell-penetrating peptide mechanisms of action for membrane interaction, cellular uptake, and translocation utilizing the hydrophobic counter-anion pyrenebutyrate, BBA-Biomembr. 1788 (2009) 2509–2517.
[24] S. Futaki, W. Ohashi, T. Suzuki, et al., Stearylated arginine-rich peptides: a new class of transfection systems, Bioconjug. Chem. 12 (2001) 1005–1011.
[25] M. Anko, J. Majhenc, K. Kogej, et al., Influence of stearyl and trifluoromethylquinoline modifications of the cell penetrating peptide TP10 on its interaction with a lipid membrane, BBA-Biomembr. 1818 (2012) 915–924.
[26] N. Oskolkov, P. Arukuusk, D. Copolovici, et al., NickFects, phosphorylated derivatives of Transportan 10 for cellular delivery of oligonucleotides, Int. J. Pept. Res. Ther. 17 (2011) 147–157.
[27] P. Arukuusk, L. Pärnaste, N. Oskolkov, et al., New generation of efficient peptide-based vectors, NickFects, for the delivery of nucleic acids, BBA-Biomembr. 1828 (2013) 1365–1373.
[28] P. Arukuusk, L. Pärnaste, H. Margus, et al., Differential endosomal pathways for radically modified peptide vectors, Bioconjug. Chem. 24 (2013) 1721–1732.
[29] D. Huang, N. Korolev, K.D. Eom, et al., Design and biophysical characterization of novel polycationic epsilon-peptides for DNA compaction and delivery, Biomacromolecules 9 (2008) 321–330.
[30] E. Ramsay, M. Gumbleton, Polylysine and polyornithine gene transfer complexes: a study of complex stability and cellular uptake as a basis for their differential in-vitro transfection efficiency, J. Drug Target. 10 (2002) 1–9.
[31] K. Ezzat, S.E. Andaloussi, E.M. Zaghloul, et al., PepFect 14, a novel cell-penetrating peptide for oligonucleotide delivery in solution and as solid formulation, Nucleic Acids Res. 39 (2011) 5284–5298.
[32] J. Regberg, A. Srimanee, M. Erlandsson, et al., Rational design of a series of novel amphipathic cell-penetrating peptides, Int. J. Pharm. 464 (2014) 111–116.
[33] C. Bechara, S. Sagan, Cell-penetrating peptides: 20 years later, where do we stand? FEBS Lett. 587 (2013) 1693–1702.
[34] G. Tünnemann, R.M. Martin, S. Haupt, et al., Cargo-dependent mode of uptake and bioavailability of TAT-containing proteins and peptides in living cells, FASEB J. 20 (2006) 1775–1784.
[35] J.R. Maiolo, M. Ferrer, E.A. Ottinger, Effects of cargo molecules on the cellular uptake of arginine-rich cell-penetrating epeptides, Biochim. Biophys. Acta Biomembr. 1712 (2005) 161–172.
[36] I. Nakase, M. Niwa, T. Takeuchi, et al., Cellular uptake of arginine-rich peptides: roles for macropinocytosis and actin rearrangement, Mol. Ther. 10 (2004) 1011–1022.
[37] R. Fischer, T. Waizenegger, K. Köhler, R. Brock, A quantitative validation of fluorophore-labelled cell-permeable peptide conjugates: fluorophore and cargo dependence of import, Biochim. Biophys. Acta Biomembr. 1564 (2002) 365–374.
[38] R. Fischer, M. Fotin-Mleczek, H. Hufnagel, R. Brock, Break on through to the other side — biophysics and cell biology shed light on cell-penetrating peptides, Chembiochem 6 (2005) 2126–2142.
[39] E. Bárány-Wallje, J. Gaur, P. Lundberg, et al., Differential membrane perturbation caused by the cell penetrating peptide Tp10 depending on attached cargo, FEBS Lett. 581 (2007) 2389–2393.
[40] J.M. Freire, A.S. Veiga, B.G. de la Torre, et al., Quantifying molecular partition of cell-penetrating peptide cargo supramolecular complexes into lipid membranes: optimizing peptide-based drug delivery systems, J. Pept. Sci. 19 (2013) 182–189.
[41] L.D. Mayer, M.J. Hope, P.R. Cullis, Vesicles of variable sizes produced by a rapid extrusion procedure, BBA-Biomembr. 858 (1986) 161–168.
[42] S. Provencher, A constrained regularization method for inverting data represented by linear algebraic or integral-equations, Comput. Phys. Commun. 27 (1982) 213–227.
[43] S. Provencher, CONTIN — a general-purpose constrained regularization program for inverting noisy linear algebraic and integral-equations, Comput. Phys. Commun. 27 (1982) 229–242.

[44] A. Tossi, L. Sandri, A. Giangaspero, in: E. Benedetti, C. Pedone (Eds.), Peptides: Proceedings of the 27th European Peptide Symposium, Edizioni Ziino, Naples, Italy, 2002, pp. 416–417.
[45] A. Arbuzova, G. Schwarz, Pore-forming action of mastoparan peptides on liposomes: a quantitative analysis, BBA-Biomembr. 1420 (1999) 139–152.
[46] P. Lundberg, S. El-Andaloussi, T. Sütlü, et al., Delivery of short interfering RNA using endosomolytic cell-penetrating peptides, FASEB J. 21 (2007) 2664–2671.
[47] F. Hu, S. Jiang, Y. Du, et al., Preparation and characterization of stearic acid nanostructured lipid carriers by solvent diffusion method in an aqueous system, Colloid Surf. B. 45 (2005) 167–173.
[48] R. Müller, K. Mader, S. Gohla, Solid lipid nanoparticles (SLN) for controlled drug delivery — a review of the state of the art, Eur. J. Pharm. Biopharm. 50 (2000) 161–177.
[49] R. Müller, C. Jacobs, O. Kayser, Nanosuspensions as particulate drug formulations in therapy rationale for development and what we can expect for the future, Adv. Drug Deliv. Rev. 47 (2001) 3–19.
[50] S.H. Kang, M.J. Cho, R. Kole, Up-regulation of luciferase gene expression with antisense oligonucleotides: implications and applications in functional assay developments, Biochemistry 37 (1998) 6235–6239.
[51] S. Elbashir, J. Harborth, W. Lendeckel, et al., Duplexes of 21-nucleotide RNAs mediate RNA interference in cultured mammalian cells, Nature 411 (2001) 494–498.
[52] A.J. Millar, S.R. Short, K. Hiratsuka, et al., Firefly luciferase as a reporter of regulated gene expression in higher plants, Plant Mol. Biol. Rep. 10 (1992) 324–337.
[53] S. Mayor, R.E. Pagano, Pathways of clathrin-independent endocytosis, Nat. Rev. Mol. Cell Biol. 8 (2007) 603–612.
[54] K. Ezzat, H. Helmfors, O. Tudoran, et al., Scavenger receptor-mediated uptake of cell-penetrating peptide nanocomplexes with oligonucleotides, FASEB J. 26 (2012) 1172–1180.